Radar Data Assimilation with JEDI LETKF for Ensemble Forecasting of Hurricane Ida (2021) Using a HAFS-Like Configuration

Chong-Chi Tong,[a*] Chengsi Liu,[a+] and Ming Xue[a,b]

[a] *Center for Analysis and Prediction of Storms, University of Oklahoma, Norman, OK 73072*

[b] *School of Meteorology, University of Oklahoma, Norman, OK 73072*

Corresponding author: Chengsi Liu, cliu@ou.edu

[*]*Current affiliation: Cooperative Institute for Research in Environmental Sciences, University of Colorado Boulder, Boulder, Colorado, and NOAA/Physical Sciences Laboratory, Boulder, Colorado*

[+]*Current affiliation: Cooperative Institute for Severe and High-Impact Weather Research and Operations, University of Oklahoma, Norman, Oklahoma, and NOAA/National Severe Storms Laboratory, Norman, Oklahoma*

Submitted to Monthly Weather Review

Accepted. March 19, 2026

ABSTRACT

This study evaluates the capability of the Local Ensemble Transform Kalman Filter within the Joint Effort for Data Assimilation Integration (JEDI) framework to directly assimilate radar observations for improving short-range ensemble forecasts of landfalling hurricanes. Experiments are performed using a model configuration that adopts the physics suite of the Hurricane Analysis and Forecast System (HAFS) for Hurricane Ida (2021). Four hourly cycling data assimilation (DA) experiments are conducted and compared against a control forecast without DA. The baseline DA experiment assimilates only conventional observations, while the other three additionally assimilate radar reflectivity from the Multi-Radar Multi-Sensor system, radial velocity from WSR-88D radars, or both. Results show that assimilating radial velocity substantially improves the inner-core wind structure, reduces the ensemble spread in track forecasts during the DA cycling, and enhances the accuracy of landfall location forecasts. Assimilating reflectivity improves rainfall forecasts, particularly for outer rainbands prior to landfall, while having relatively minor impact on intensity. Post-landfall rainfall prediction also benefits from radial velocity assimilation, mainly through improved track forecasts. Quantitative verification using equitable threat scores shows that radar DA improves forecasts of total rainfall accumulation. Radial velocity assimilation contributes most to moderate rainfall prediction, while reflectivity assimilation offers greater skill in forecasting extreme rainfall. These findings underscore the value of incorporating radar data into ensemble hurricane forecasting and provide practical guidance for future implementation of radar DA within the HAFS-JEDI framework for operational applications.

1. Introduction

Tropical cyclone (TC) forecasting is crucial for mitigating the devastating impacts on communities, infrastructure, economies, and ecosystems, especially when strong TCs, i.e., hurricanes or typhoons, make landfall. Accurate forecasts of TC track, intensity, and structure are essential for timely evacuations, emergency response, and optimal resource allocation. In recent decades, considerable progress in TC forecasting have been achieved through advancements in numerical weather prediction (NWP) models (e.g., Alaka et al. 2024; Chen et al. 2007; Davis et al. 2008; Fierro et al. 2009), improved data assimilation (DA) approaches, and use of observations from an increasing variety of platforms (e.g., Dong and Xue 2013; Green et al. 2022; Hsiao et al. 2012; Weng and Zhang 2012; Zhang et al. 2009; Zhang and Pu 2019; Zhao and Xue 2009). Despite these improvements, accurately predicting the complex evolution of TC inner-core structures and rapid intensity changes remains challenging, underscoring the need for continuous development in high-resolution modeling and sophisticated DA systems. NOAA's ongoing development of the Hurricane Analysis and Forecast System (HAFS) represents a significant effort toward addressing these challenges and enhancing operational hurricane forecasting capabilities.

Developed as the TC component of NOAA's Unified Forecast System (UFS) based on the FV3 dynamic core (Putman and Lin 2007), HAFS aims to provide more reliable and skillful guidance for hurricane forecasting by leveraging high-resolution modeling and advanced DA techniques. Before its first operational implementation in June 2023, HAFS underwent extensive development and real-time testing. Compared to previous operational hurricane forecast models such as the Hurricane Weather Research and Forecasting model and the Hurricanes in a Multi-scale Ocean-coupled Non-hydrostatic model (HMON), HAFS has demonstrated improved accuracy in track forecasts, notably reducing cross-track errors (Dong et al. 2020; Hazelton et al. 2023; Hazelton et al. 2021). However, challenges remain, particularly regarding intensity prediction, primarily due to limitations such as coarser horizontal resolution and insufficient inner-core data assimilation. Addressing these challenges remains critical to further enhancing HAFS's predictive capabilities.

HAFS currently employs the Gridpoint Statistical Interpolation (GSI; Wu et al. 2002) system for data assimilation, performing inner-core analysis using the First Guess at Appropriate Time (FGAT; Pondeca et al. 2011) and assimilating the set of observations used in the Global Forecast System (GFS) through the four-dimensional hybrid ensemble-variational (4DEnVAR). It also incorporates vortex initialization (VI; Kurihara et al. 1993) technique adopted from the operational HWRF including vortex relocation and intensity-based vortex modification (Lu et al. 2017).

Towards the goal of unifying DA for all NOAA's operational forecasting systems, and modernizing the DA infrastructure, NOAA plans to transition the DA component of HAFS to the Joint Effort for Data Assimilation Integration (JEDI; Tremolet and Auligne 2020), a community-based DA framework selected for the UFS (Jacobs 2021; Uccellini et al. 2022). JEDI is designed as a modular, model-agnostic DA framework that supports coupled Earth system modeling, accelerates the transition from research to operations, and is scalable across diverse computing platforms. Although its application to hurricane forecasting remains in the early stages, recent work, such as Liu et al. (2023), has demonstrated the potential benefits of JEDI by assimilating satellite and ocean observations, indirectly improving hurricane forecasts through improved initialization of ocean state variables; consistent findings are reported by Kim et al. (2014) with HWRF.

Radar observations, especially from the Next Generation Weather Radar (NEXRAD) network in coastal areas, provide high-resolution data for capturing detailed TC structures and wind field characteristics, particularly near landfall. Numerous studies (e.g., Dong and Xue 2013; Zhang et al. 2009; Zhao and Xue 2009) have demonstrated significant improvements in TC forecasts through the assimilation of radar reflectivity and radial velocity data into convection-permitting models using various DA methods, such as the 3-dimensional variational (3DVAR) method and the ensemble Kalman filter (EnKF). These improvements include more accurate analyses of TC inner-core structures and reduced errors in subsequent track and intensity forecasts, achieved without relying on bogus vortex procedures. Recent studies (e.g., Li et al. 2024; Wang and Pu 2021) have further confirmed the benefits of radar DA in operational hurricane forecasting systems such as HWRF, utilizing hybrid 3DEnVar of GSI. For future version of operational HAFS, there is need to implement and test radar DA capabilities within JEDI, and further examine the impact of the data on TC forecasting. This has not been done so far, at least in the published literature.

Building on our prior work (Park et al. 2023), where we successfully implemented and tested radar DA capabilities within the JEDI ensemble DA framework coupled with FV3-LAM for continental convection forecasting, this study extends it to tropical cyclone forecasting. It presents the first effort to evaluate the impact of radar DA using JEDI on hurricane analysis and forecasting. Specifically, we use the JEDI Local Ensemble Transform Kalman Filter (LETKF) coupled with an FV3 limited-area model configured with the physics suite employed by the operational HAFS. This work aims to establish initial radar DA capabilities within JEDI for potential future adoption within operational HAFS, and at the same time to examine the impact of assimilating such data on forecasting a landfalling hurricane, that is covered by the coastal operational WSR-88D radars when it gets close to the coast.

The rest of the paper is organized as follows. Section 2 provides a brief introduction to the studied case of Hurricane Ida. The forecast model, data assimilation method, observations, and the experimental setup are described in section 3. Section 4 presents the experiment results, including detailed discussions of the data impact on both analyses and forecasts for key hurricane features. Finally, key findings are summarized in section 5, together with discussions about potential future work.

2. Case Overview: Hurricane Ida (2021)

Hurricane Ida originated as a tropical depression near 1200 UTC on 26 August 2021, approximately 280 km southwest of Kingston, Jamaica. A rapid intensification process was observed starting at 1200 UTC 28 August, with favorable conditions including light vertical wind shear and warm sea surface temperature as it passes over the Gulf of Mexico. Over a 24-h period of rapid strengthening, the maximum sustained winds increased from 35 to 65 m s^{-1}, while the central pressure decreased from 986 to 929 hPa. Steered by the flow on the southwestern side of the subtropical ridge, Hurricane Ida continuously moved northwestward and made landfall at Port Fourchon, Louisiana at 1655 UTC 29 August as a category 4 hurricane with a 130-kt (i.e., ~65 m s^{-1}) intensity, which is one of the three strongest hurricanes on record that made landfall in Louisiana west of the Mouth of the Mississippi River, other than Hurricane Laura (2020) and the Last Island Hurricane (1856). Ida also brought record-breaking rainfall and subsequent flooding to multiple states, including Louisiana, Mississippi, Tennessee, and the Northeastern United States. According to the TC report issued by the National Hurricane Center (NHC, 2022: Tropical cyclone report. Accessed 30 September 2025, https://www.nhc.noaa.gov/data/tcr/AL092021_Ida.pdf), the resultant devastation, attributable to the winds, rainfall, storm surges, and tornadoes, led to an aggregate of $75 billion in national

damages and 55 direct and 32 indirect fatalities. The best track of Hurricane Ida along its lifespan is shown in Fig. 1.

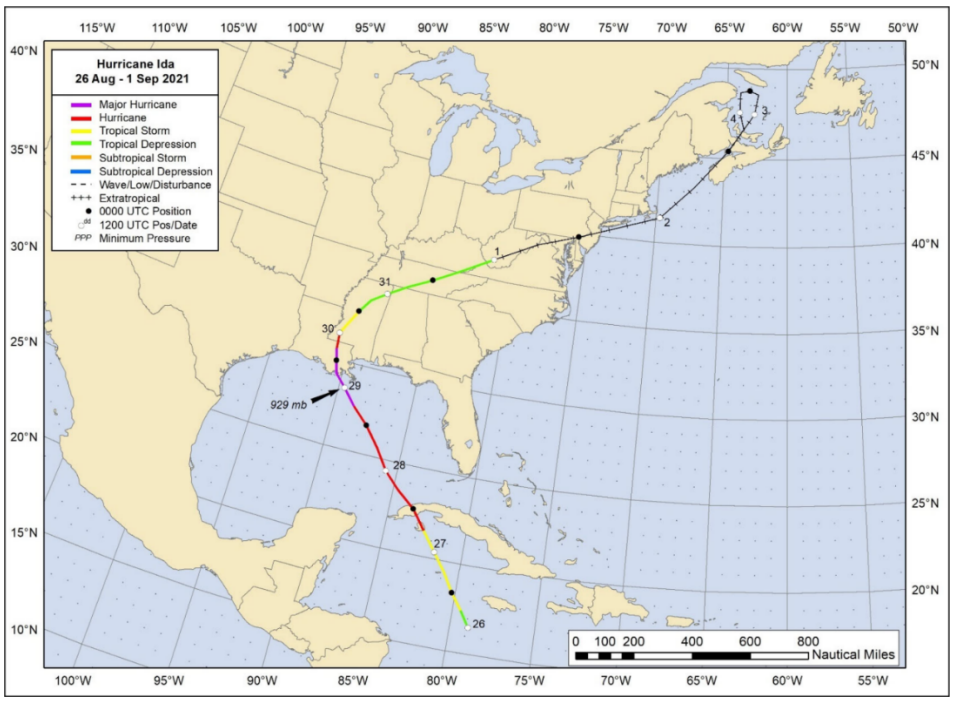

FIG. 1. Best track of Hurricane Ida, 26 August to 1 September 2021 (courtesy of NOAA National Hurricane Center). The black arrow denotes where the lowest surface center pressure 929 hPa occurred during the lifetime of Hurricane Ida.

3. Prediction model, observations, and data assimilation experiment design

a. Prediction model and simulation setup

The prediction model used in this study is the UFS Short-Rang Weather Application (SRW App) v2.0.0, a community-based Earth modeling system based on the FV3 dynamical core and designed as an operational application for HAFS. Our simulations utilize FV3_GFS_v16 physical suite through the Common Community Physics Package (CCPP), consisting of the GFS Rapid Radiative Transfer Model for Global Circulation Models (RRTMG, Mlawer et al. 1997), the GFS Noah Multi-Physics Land Surface Model (LSM; Niu et al. 2011), the GFS scale-aware TKE-Eddy Diffusivity Mass Flux (sa-TKE-EDMF) PBL scheme (Han and Bretherton 2019), the GFS scale-aware Simplified Arakawa-Schubert (sa-SAS) schemes for deep and shallow convection (Arakawa and Schubert 1974), and the single-moment Geophysical Fluid Dynamics Laboratory (GFDL) cloud microphysics scheme (Lord et al. 1984).

The prognostic state variables include three wind velocity components (u, v, and w), sensible temperature (T), pressure (p, in a form of "*delp*", the thickness between two adjacent model levels), specific humidity (q), and hydrometeor mixing ratios (cloud water, cloud ice, rain, snow, and graupel). The simulation domain is centered over Alabama, consisting of 1050 × 850 grid cells with a 3-km horizontal resolution (Fig. 2). In vertical direction, a 64-level hybrid coordinate is utilized, with a terrain-following bottom, isobaric upper levels, and a model top at 40 Pa.

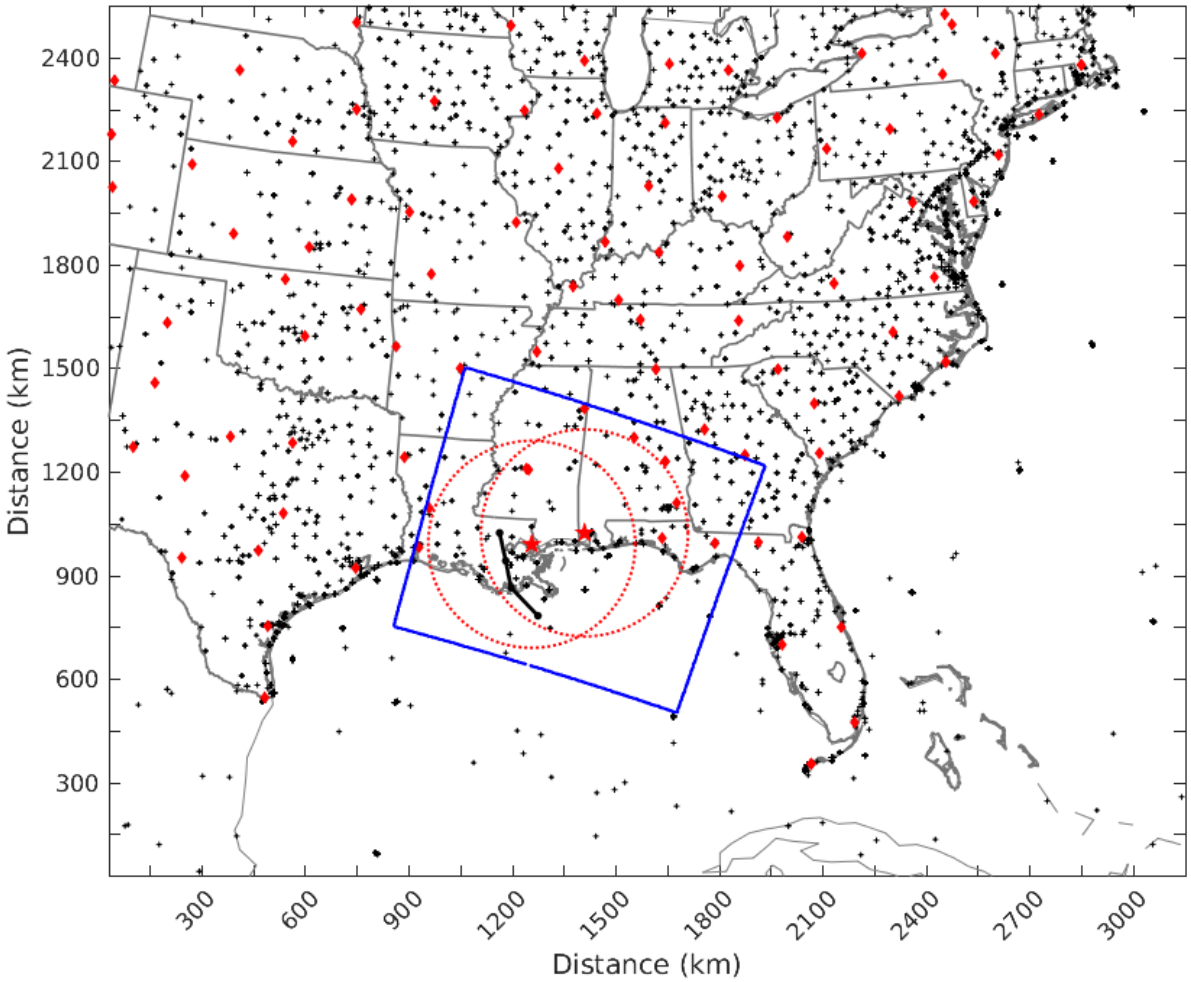

FIG. 2. Physical domain for simulation, the WSR-88D radars (including the coastal KMOB and KLIX marked by red pentagrams with dotted circles indicating their radial velocity coverage at the lowest elevation angles, and other sites in red diamonds), conventional surface observation sites available at 1200 UTC 29 August (black crosses), and the 6-hourly best track of Ida between 1200 UTC 29 August and 0600 UTC 30 August 2021 (black dots). The sub-domain for precipitation verification is denoted by the blue rectangle.

b. Experiments design and data assimilation

A series of experiments are performed to examine the impact of assimilating different observations on hurricane ensemble forecasting. Ensemble forecasts initialized from the 0.5° Global Ensemble Forecast System (GEFS) 30-member analyses at 0600 UTC 29 August 2021 without any DA are conducted as a control experiment (hereafter refer to as NODA). Four hourly cycled DA experiments, ExpC, ExpCZ, ExpCV, and ExpCZV, are conducted on the 3-km grid between 1200 and 1500 UTC, starting from a 6-h spin-up ensemble. The experiments differed in the set of assimilated observations, as summarized in Table 1. The assimilated conventional data include radiosonde, VAD winds, surface observations, and commercial aircraft reports. In addition, reconnaissance flights provide valuable dropsonde profiles in the open ocean around the hurricane, where surface observations are limited. For radar observations, the 33-level composite reflectivity (Z) from the Multi-Radar Multi-Sensor (MRMS) dataset with established quality control (Zhang et al. 2016) is utilized, along with Level-II radial velocity (V_r) from individual WSR-88D radars located within the model domain (Fig. 2). After de-aliasing to remove velocity folding, the V_r observations are horizontally

interpolated onto the 3-km model grid using a local least-square fitting procedure, while retaining their original radar elevation levels in the vertical (Gao et al. 2006). This process effectively thins the native radar observations to the model grid scale, while still assuming a diagonal observation error covariance. The cycling DA ending at 1500 UTC leaves approximately a 2-hour lead time before Hurricane Ida's landfall at 1655 UTC. After all DA cycles are completed, ensemble forecasts are initialized from the final ensemble analyses at 1500 UTC and run for 15 hours. Lateral boundary conditions are provided by 3-hourly ensemble forecasts from the 1200 UTC cycle GEFS. The timeline of the experiments is illustrated in Fig. 3. It is worth noting that under the cycling setup, NODA has a lead time 9 hours longer than all DA experiments.

Table 1. DA experiments and assimilated observations.

Name	*Conventional Data*	*Reflectivity*	*Radial Velocity*
ExpC	Yes	No	No
ExpCZ	Yes	Yes	No
ExpCV	Yes	No	Yes
ExpCZV	Yes	Yes	Yes

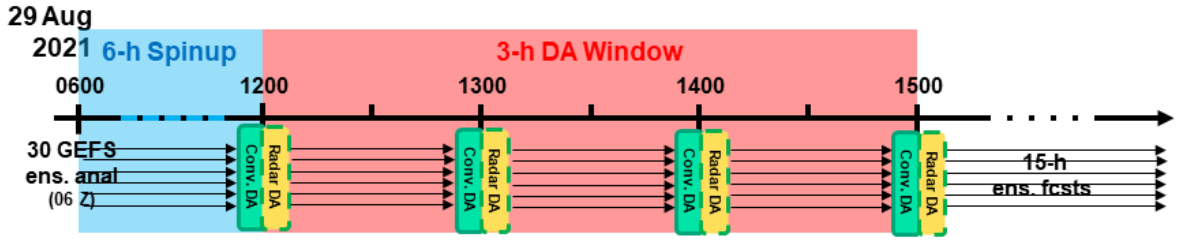

FIG. 3. Flowchart of the cycled DA experiments. Hourly ensemble DA cycles are run from 1200 through 1500 UTC, assimilating different data among the experiments, and 15-h ensemble forecasts are launched from the final analyses at 1500 UTC.

The LETKF method (Hunt et al. 2007) in JEDI is used for the DA experiments. Conventional observations of surface pressure, winds, temperature, and humidity are assimilated, and corresponding model state variables are updated. LETKF utilizes an observation error-based covariance localization method, in which covariances are scaled according to the distance between observations and the updated grid-points (Miyoshi et al. 2007). For the assimilation of conventional observations, a horizontal localization radius of 300 km is applied using the Gaspari-Cohn correlation function (Gaspari and Cohn 1999). The vertical localization follows Park et al. (2023) with a radius of 0.7 in a natural logarithmic pressure unit. For radar observations, a much tighter horizontal localization radius of 18-km is applied for assimilating reflectivity, aiming to confine its impact near precipitation regions (Labriola et al. 2021; Park et al. 2023; Snook et al. 2015). For radial velocity assimilation, a larger horizontal localization radius of 90 km is employed to allow the radial velocity data to have a broader influence on the hurricane vortex; this length scale is adopted in Zhang et al. (2009) using the successive covariance localization technique for assimilating sub-sampled radar observations for hurricane initialization. Vertically, a reduced localization radius of 0.4 natural logarithmic p is utilized for all radar observations; this deliberate choice is based on our sensitivity test result (not shown) found to best preserve the vortex structures.

When assimilating radar observations, the updated state variables include the three wind components (u, v, w), temperature (T), specific humidity (q), and all hydrometeor mixing ratios (q_x). For reflectivity, the microphysics-scheme-dependent forward operator in JEDI (Park et al.

2023) computes simulated Z from the model hydrometeors, enabling consistent mapping of analysis increments between observation space and the corresponding model variables. Following Park et al. (2023), the observation error standard deviations are assumed to be 5 dBZ for Z and 3 m s^{-1} for Vr. Pressure is not updated by radar data to avoid significant small-scale surface pressure deviations from the results of conventional observation DA that negatively impact forecasting in additional sensitivity tests (not shown). To mitigate the ensemble under-dispersion issue, a relaxation-to-prior-spread (RTPS; Whitaker and Hamill 2012) procedure is applied at each assimilation cycle. This procedure restores the ensemble spread of the analysis to 95% of the background spread, helping preserve ensemble spread throughout the DA cycles.

4. Results

a. Impact of data assimilation on the analysis

The near-surface analyses of the horizontal wind and pressure from the first cycle are compared against the forecast background in Figure 4, alongside the lowest-tile reflectivity and radial velocity observed by KLIX, the nearest coastal radar to the storm. The results from the first ensemble member are used as an example for general discussions. We show an ensemble member instead of an ensemble average here because the ensemble average tends to smooth structure details when there are offsets in the hurricane center locations among the members.

Compared to the background forecast (Fig. 4c), the ExpC analysis (Fig. 4d) exhibits significant adjustments in both wind and pressure fields due to the assimilation of conventional observations. Specifically, the low-level wind profiles provided by the dropsondes around the storm center (denoted in Figs. 4d-g) account for the primary wind corrections. Besides, other observations, such as surface pressure, temperature, and humidity, from nearby surface stations can also contribute to the analysis updates through the ensemble-derived cross-covariances utilized in the LETKF. While the general hurricane location remains similar to the background, the calm region within the eye shrinks and the minimum pressure near the center decreases. The circulation around the hurricane center also strengthens, with the greatest wind intensification found along the east and south sides.

Assimilating additional reflectivity data produces only minor changes in the analyzed circulation, as seen in the comparison between Figs. 4d and 4e, suggesting relatively weak or spatially limited correlations between reflectivity and kinematic wind fields. The pressure field remains unchanged because it is not updated during the radar DA process. As shown in Figs. 4a-b, at 1200 UTC, the hurricane was still located far from the nearest coastal radar capable of observing it. Most of the available data are located near the outer edge of the effective radar coverage area and therefore at relatively high altitudes (e.g., above 4 km for the lowest elevation angle at 200 km away from the radar). As a result, ExpCV (Fig. 4f) and ExpCZV (Fig. 4g) show only slight enhancements in the surface circulation, mainly in the northeast quadrant of the hurricane, compared to ExpC (Fig. 4d) and ExpCZ (Fig. 4e) that do not assimilate V_r data.

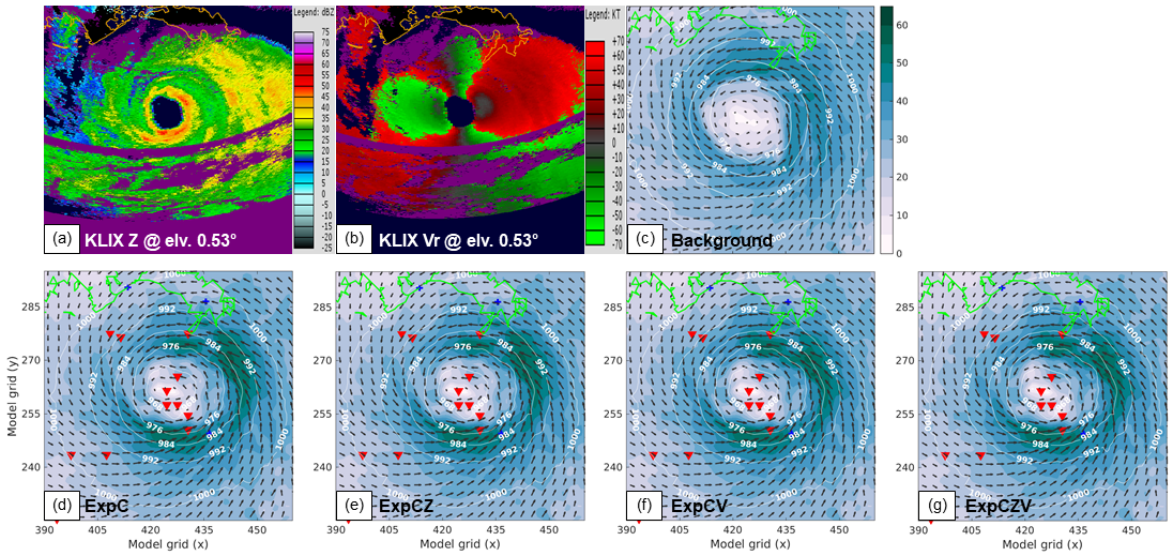

FIG. 4. KLIX Level-II raw observed (a) radar reflectivity (dBZ) and (b) radial velocity (knot) at the lowest elevation angel (0.53°) at 1201 UTC. Horizontal wind vectors and speed (color shaded, m s^{-1}) and pressure (white contours in an interval of -8 hPa, starting from 1000 hPa) at the first model level above ground (~47 m at the Hurricane region) at 1200 UTC for the first ensemble member (c) background forecast (launched from the GEFS 0600 UTC analysis), and the first cycle analyses from experiments (d) ExpC, (e) ExpCZ, (f) ExpCV, and (g) ExpCZV. The locations of surface stations and dropsondes available at this time are denoted by blue crosses and red inverted triangles, respectively.

Figure 5 shows ensemble-averaged azimuthal-mean radius-height cross sections that depict the axisymmetric structure of the analyzed hurricane at 1200 UTC. The ensemble mean is used here to facilitate a statistically robust assessment of the relative performance of different experiments in depicting TC structures; while smoothing is acknowledged, it is common to all experiments and should not bias the comparisons. To produce these cross sections, the forecasts from all ensemble members are first aligned by the location of their minimum surface pressure. The variables of interest are then averaged azimuthally over 360° as a function of radius from the aligned storm center followed by ensemble-average at each model level. The top row of Fig. 5 shows the tangential wind and the horizontal temperature anomaly, while the bottom row shows radial wind and vertical velocity. The temperature anomaly is calculated as the deviation from the mean horizontal temperature within a 240-km radius.

Consistent with the surface horizontal circulation shown in Fig. 4, the ExpC and ExpCZ analyses exhibit moderately stronger low-level tangential winds (Figs. 5b and c) and considerably enhanced radial inflow near the surface (Figs. 5g and h) compared to the background (Figs. 5a and f), primarily due to the assimilation of conventional observations. In addition, both experiments analyze a significantly stronger warm core below 5 km AGL within the eye, indicating improved thermal structure associated with enhanced low-level circulation.

When reflectivity data are additionally assimilated, the maximum updraft shifts closer to the inner core (Fig. 5h), suggesting a tighter vortex structure. In contrast, assimilation of radial velocity produces a more substantial enhancement of inner-core circulation. In ExpCV and ExpCZV (Figs. 5d and e), the tangential winds are not only enhanced near the surface but also intensified significantly at upper levels, forming a deeper and more vertically coherent vortex structure compared to ExpC and ExpCZ (Figs. 5b and 5c). The apparent “reverse-stadium” shape of the eyewall aloft primarily reflects the vertical sampling limits of radar observations, given the nearest radar providing little coverage below ~4 km altitude at its lowest tilt; flow corrections blow therefore rely solely on conventional data, which are relatively sparse as

implied in ExpC. Along with the tighter inner core inferred from the tangential winds, the warm core extends upward to about 12 km AGL. Both ExpCV and ExpCZV analyze stronger and deeper updrafts confined mostly around the narrowed eyewall (Fig. 5i and j), with a slightly narrower updraft region produced by ExpCZV.

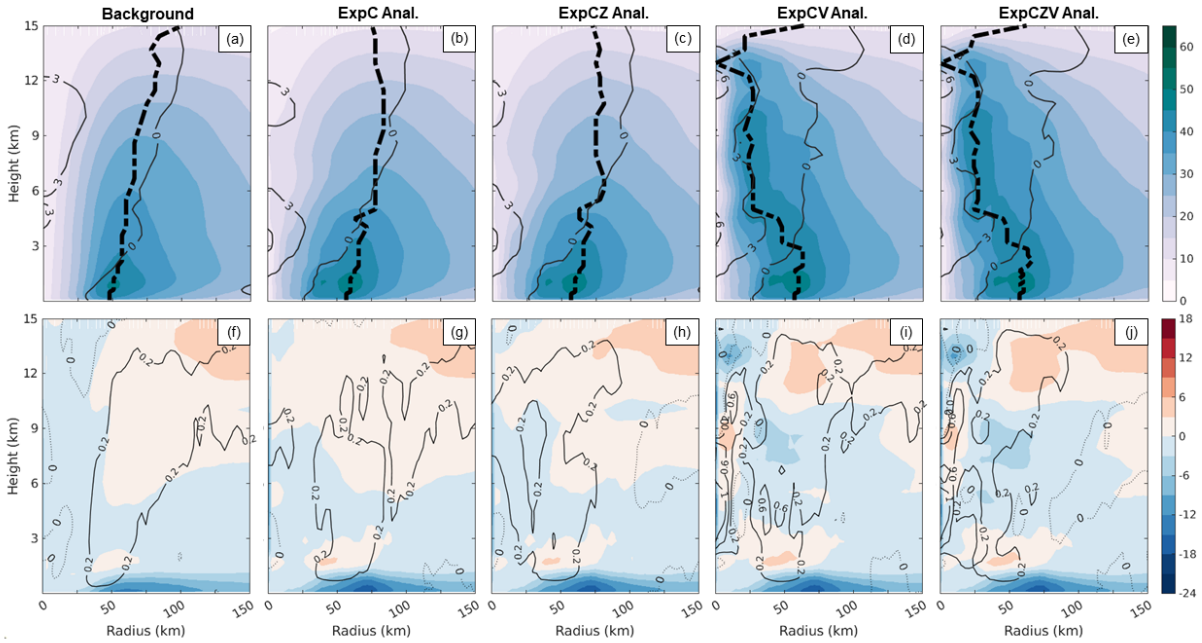

FIG. 5. Azimuthal-mean radius-height cross sections at 1200 UTC for (a), (f) the background forecast and first-cycle analyses from (b), (g) ExpC, (c), (h) ExpCZ, (d), (i) ExpCV, and (e), (j) ExpCZV. Top row shows tangential wind speed (color shaded, m s^{-1}), and temperature anomaly (thin black contours, K), and radius of maximum wind (thick dashed line). Bottom row shows radial wind speed (color shaded, m s^{-1}) and vertical velocity (black contours, m s^{-1}).

Figure 6 shows the final-cycle analyses of surface-level hurricane circulation at 1500 UTC from the first ensemble member for four DA experiments, together with the same time KLIX observations at the lowest elevation angle. After several DA cycles, all experiments produce much more contracted eyewalls compared to their first cycle analyses. Among these experiments, ExpC (Fig. 6d) exhibits the strongest maximum wind speed, with the greatest intensification occurring in the northeast quadrant, along with the most widespread intense vortex circulation. Additional assimilation of reflectivity in ExpCZ (Fig. 6e) reduces somewhat both the overall intensity of vortex and the spatial extent of maximum winds. In contrast, assimilation of radial velocity data in ExpCV or ExpCZV (Figs. 6f and 6g) leads to an even more compact and circular eyewall, characterized by a smaller radius of maximum wind (RMW). Moreover, both ExpCV and ExpCZV show comparably low minimum surface pressure among all experiments, suggesting that radial velocity assimilation is most effective at intensifying the hurricane, consistent with results of previous studies (e.g., Zhao and Xue 2009; Dong and Xue 2013).

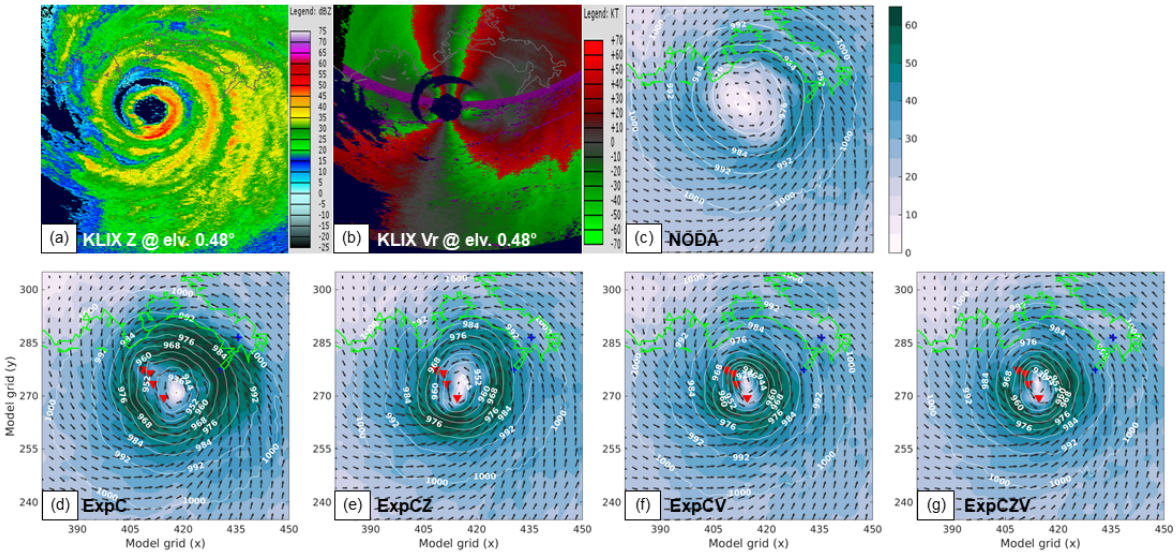

FIG. 6. As in Fig. 4, but for (a), (b) the lowest elevation angle observations of KLIX at 1500 UTC, (c) NODA forecast and the final cycle analyses at 1500 UTC for (d) ExpC, (e) ExpCZ, (f) ExpCV, and (g) ExpCZV.

The vertical structures of the final analyses at 1500 UTC are shown in Fig. 7. Among all experiments, ExpC exhibits the strongest maximum tangential winds at lower levels, consistent with the surface level analysis shown previously (Fig. 6d). Similar to the first cycle analyses discussed earlier, both ExpC and ExpCZ (Fig. 7b, c) again display a relatively shallow layer of intense tangential winds along the eyewall compared to the experiments assimilating radial velocity (ExpCV and ExpCZV). Specifically, the tangential wind exceeding 30 m s^{-1} in the former is mostly confined below 9 km in ExpC and ExpCZ, whereas they reach heights near 13 km in ExpCV and ExpCZV (Figs. 7d, e). In addition, ExpCV and ExpCZV show a significantly deeper vortex structure, with maximum temperature anomalies located above 10 km altitude. The RMW (denoted by the thick dashed lines) is also reduced in ExpCV and ExpCZV, indicating a more compact eyewall structure.

For the vertical motion, both ExpCV and ExpCZV (Figs. 7i, j) produce substantially stronger updraft closely aligned with the RMW axis. In the contrast, without assimilating radial velocity, the updraft intensity in ExpC and ExpCZ shows limited strengthening compared to the first cycle analyses. It is worth noting that ExpCZ exhibits discontinuity in the updraft structure between 5 and 11 km (Fig. 7h). Such a discontinuity is inferred not to result from the direct reflectivity assimilation, as it is not seen in the first cycle (Fig. 5h). Instead, its appearance after multiple cycles suggests that some incoherence may arise in the model dynamics during the forecast, responding to the hydrometeor and thermodynamic adjustments introduced by assimilating reflectivity alone, in the absence of direct kinematic constraints.

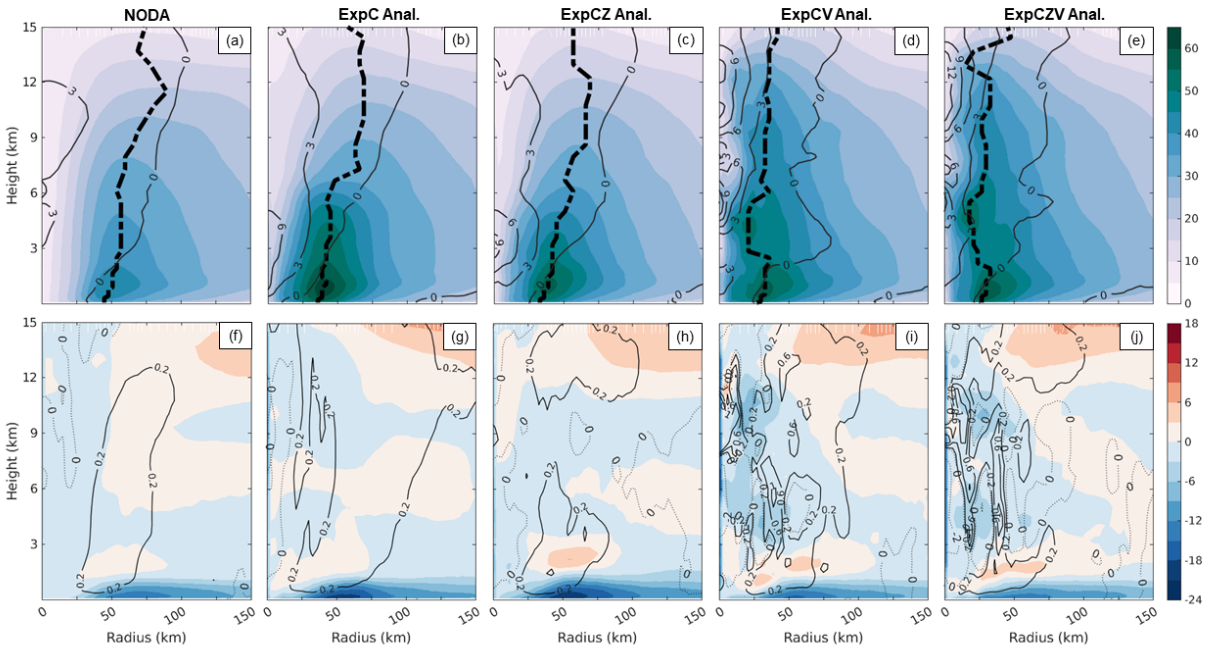

FIG. 7. As in Fig. 5, but for (a), (f) NODA forecast and the final cycle analyses at 1500 UTC for (b), (g) ExpC, (c), (h) ExpCZ, (d), (i) ExpCV, and (e), (j) ExpCZV.

In Figure 8, the final DA cycle reflectivity analysis from the first ensemble member for different experiments are presented, illustrating the accumulated influences of designated observations interacting with model dynamics and physics through intermittent forecasts. The reflectivity is derived from the precipitating hydrometeor analysis using a diagnostic operator consistent with the microphysics scheme employed in the forecast model. At this time, the observed MRMS reflectivity (Fig. 8a) depicts a compact tropical cyclone core with a well-defined eyewall and strong convective bands at the northeast quadrant. It is worth noting that, due to the limited range of the costal radar network, lower-level reflectivity south of the storm is not captured in the MRMS field shown here. NODA (Fig. 8b) exhibits a displaced and less compact eyewall structure, with more diffuse inner-core convection compared to MRMS. Assimilation of conventional observations (i.e., ExpC, Fig. 8c) strengthens the storm circulation and convective organization, although the eyewall remains overly broad and offset from the observed location. With reflectivity assimilation, ExpCZ (Fig. 8d) substantially improvs the inner-core structure with a compact eyewall and reflectivity maxima closer to MRMS. ExpCV (Fig. 8e) enhances the overall circulation and spiral rainbands but retains a less compact and slightly displaced eyewall. Finally, the combined assimilation of reflectivity and radial velocity in ExpCZV (Fig. 8f) also captures a compact eyewall and strong convection, which is generally similar to ExpCZ, though with a slightly overestimated inner-core convective intensity. For each experiment, the root-mean-square difference (RMSD) with respect to MRMS is calculated over the domain in Figure 8, confined to grid points with observed or analyzed reflectivity greater than 5 dBZ. These quantitative results agree with the qualitative assessment, with the smallest errors in ExpCZ and ExpCZV and the largest errors in NODA and ExpC. Together, the results suggest the critical role of reflectivity assimilation in accurately representing the placement and intensity of TC convection.

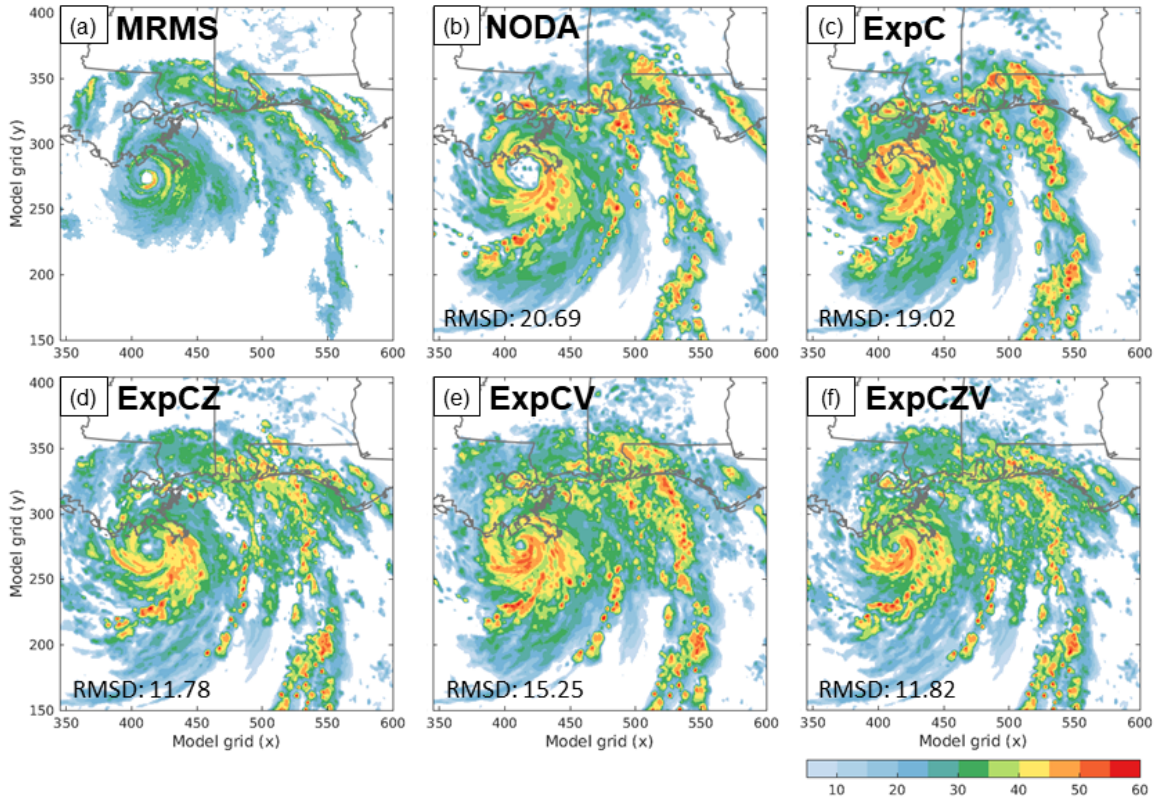

FIG. 8. Composite reflectivity analyses (dBZ) of the first ensemble member at the final DA cycle (1500 UTC) for (a) NODA, (b) ExpC, (c) ExpCZ, (d) ExpCV, and (e) ExpCZV, as compared to the (f) MRMS observations. RMSD relative to MRMS is denoted in the lower-left corner of each experiment.

Figure 9 shows the ensemble averaged minimum sea level pressures (MSLPs) from all experiments illustrating the evolution of TC intensity during the 3-h DA cycles and the subsequent 2-h forecasts near Hurricane Ida's landfall. At 1200 UTC, the background forecast significantly underpredict the TC intensity (i.e., overpredicts MSLP). The reduction of MSLP (by ~10 hPa) in the first cycle is solely due to assimilating conventional observations, as radar data are not directly used to update pressure fields. During the cycling DA, all DA experiments show substantial improvements in the TC intensity relative to the NODA, with significant reductions in MSLP. Among these experiments, ExpCV and ExpCZV exhibit significantly more rapid intensification, as indicated by lower MSLPs in the final analyses. This result suggests that assimilating radial velocity observations substantially improve the analyzed TC intensity. Following the DA cycles, the evolution of MSLP during the subsequent 2-h forecasts is further analyzed below.

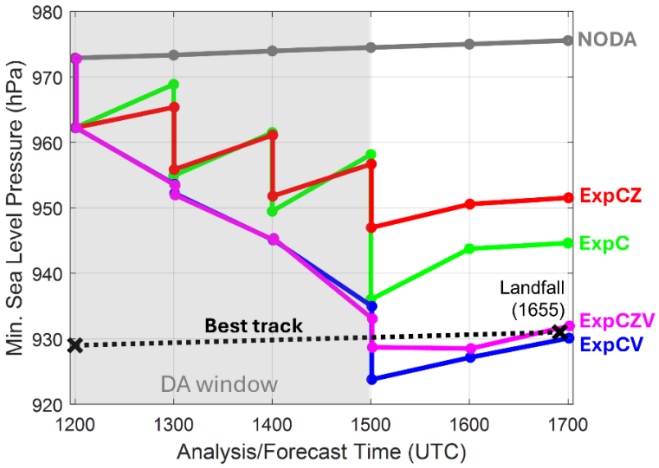

FIG. 9. Ensemble averaged minimum sea level pressure (MSLP) during 3-h cycling DA (shaded) and the subsequent 2-h forecast for all experiments. Best track MSLPs at 1200 UTC and at landfall (1655 UTC) are denoted by black crosses.

b. Impact of data assimilation on the ensemble forecasts

1) TRACK AND INTENSITY FORECASTING EVALUATION

Figure 9 also shows the ensemble forecasts of MSLP initialized from the final-cycle analyses (after 1500 UTC). During the subsequent 2-h forecast period, all experiments show a general increase in MSLP, indicating gradual weakening of the TC as it approaches landfall. Among these forecasts, the experiments assimilating radial velocity data (ExpCV and ExpCZV) exhibit MSLP values most consistent with the best track observations at the actual landfall time (1655 UTC). This result highlights the beneficial impact of radial velocity assimilation in maintaining accurate short-term intensity forecasts. In contrast, ExpCZ, which assimilates reflectivity but not radial velocity, produces the largest overestimation of MSLP (i.e., the weakest forecasted TC intensity) at landfall. This further supports earlier conclusions (discussed in section 4a) that reflectivity assimilation alone, without radial velocity data, may hinder accurate intensity forecasts.

In addition to intensity, accurate prediction of the TC track, particularly the landfall location, is critical for effective emergency responses. Figure 10 compares ensemble forecast hurricane positions at 1700 UTC (5 minutes after the observed landfall at 1655 UTC) with the best track location. Compared to NODA and ExpC, assimilating radar data (ExpCZ, ExpCV, and ExpCZV) reduces the spatial spread of the forecast TC positions, improving forecast consistency among ensemble members. Specifically, the experiments assimilating radial velocity (ExpCV and ExpCZV) exhibit significantly smaller dispersion and the smallest displacement errors, as indicated by their ensemble-averaged locations. Notably, radial velocity assimilation also reduces the bias towards the southern offshore region seen in NODA and ExpC, resulting in more ensemble members predicting the TC's landfall closer to the actual observed location.

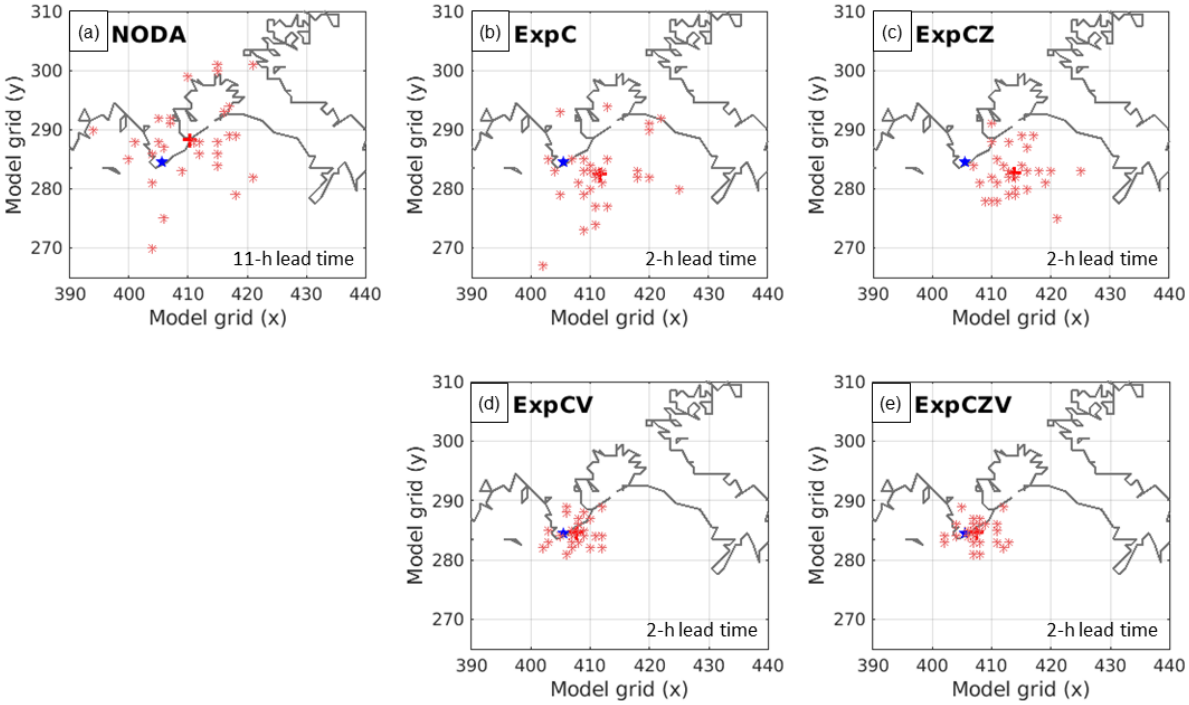

FIG. 10. Ensemble forecast hurricane locations (red asterisks) valid at 1700 UTC 29 August 2021 (5 minutes after the observed landfall) for (a) NODA, (b) ExpC, (c) ExpCZ, (d) ExpCV, and (e) ExpCZV. Ensemble-averaged locations and best track landfall locations are denoted by bold red crosses and blue pentagrams, respectively. The lead time at this valid hour is noted in the lower right corner of each panel.

Figure 11a-b show the ensemble-averaged track forecasts starting at 1800 UTC 29 August (about one hour after the landfall), verified against the 6-hourly best track data through 0600 UTC 30 August. All experiments exhibit a systematic rightward (eastward) bias in their track forecasts relative to the best track, consistent with the "right-of-track" bias previously identified in multiple-case statistics (Dong et al. 2020; Hazelton et al. 2022). Initially, both ExpCV and ExpCZV provide more accurate tracks than other experiments, reducing track errors by approximately 12 km compared with NODA (Fig. 11b), with their performance differences remaining well within the shaded ranges that indicate 95% confidence intervals derived from 5,000 bootstrap samples. In contrast, experiments without assimilating radial velocity (ExpC and ExpCZ) shows larger eastward deviations. By 0600 UTC, ExpCV continues to yield the smallest track error (~20 km), while ExpCZV experiences increased errors due to a slower northward movement. Overall, radar data assimilation, particularly radial velocity assimilation, improves short-term hurricane track forecasts following landfall, aligning with previous findings (e.g., Zhao and Xue 2009; Dong and Xue 2013); in the longer forecast ranges, the systematic track bias across all experiments suggests model physics as the dominant factor over DA.

The forecasts of MSLP and the maximum surface wind speed (MSW) during the 12-h post-landfall period are shown in Fig. 11c-d. NODA significantly underpredicts hurricane intensity, overestimating MSLP by about 40 hPa and underestimating MSW approximately 30 m s^{-1} at 1800 UTC. In contrast, the DA experiments, particularly ExpCV and ExpCZV, produce MSLP forecasts much closer to the best track, with initial errors within 5 hPa. ExpC and ExpCZ also show notable improvement over NODA, with 20~25 hPa lower MSLPs and ExpC slightly outperforming ExpCZ throughout the period. During the first 6 hours, observations indicate a relatively stable and gradual weakening of the hurricane (MSLP increases slowly by

about 5–10 hPa), which all DA experiments successfully capture. In contrast, NODA shows little change in MSLP during this period. Overall, the non-overlapping 95% confidence intervals suggest statistically significant improvement of all DA experiments over NODA.

Figure 11d shows that all experiments consistently underpredict the MSW throughout the forecast period. At 1800 UTC, NODA substantially underestimated MSW approximately 30 m s^{-1}. Assimilating radar data reduces this underestimation by about 10-15 m s^{-1}. Among all DA experiments, ExpCZ shows slightly lower MSW, aligning with its higher MSLP forecast. Throughout the 12-h evaluation period, the differences in MSW forecasts among the DA experiments remain relatively small and all successfully capture the observed weakening trend. By 0600 UTC, ExpC shows the largest reduction in MSW, resulting in the greatest underprediction, whereas ExpCZ exhibits the smallest weakening rate and least underprediction. By the end of the forecast period, all DA experiment reduce the MSW forecast errors to within approximately 15 m s^{-1}. It is worth noting that instead of DA impact, there are other factors responsible for the universal MSW underestimation, including the limit of 3-km resolution in resolving sharp wind gradients around the eyewall and the model physics parameterizations governing boundary layer processes and surface fluxes.

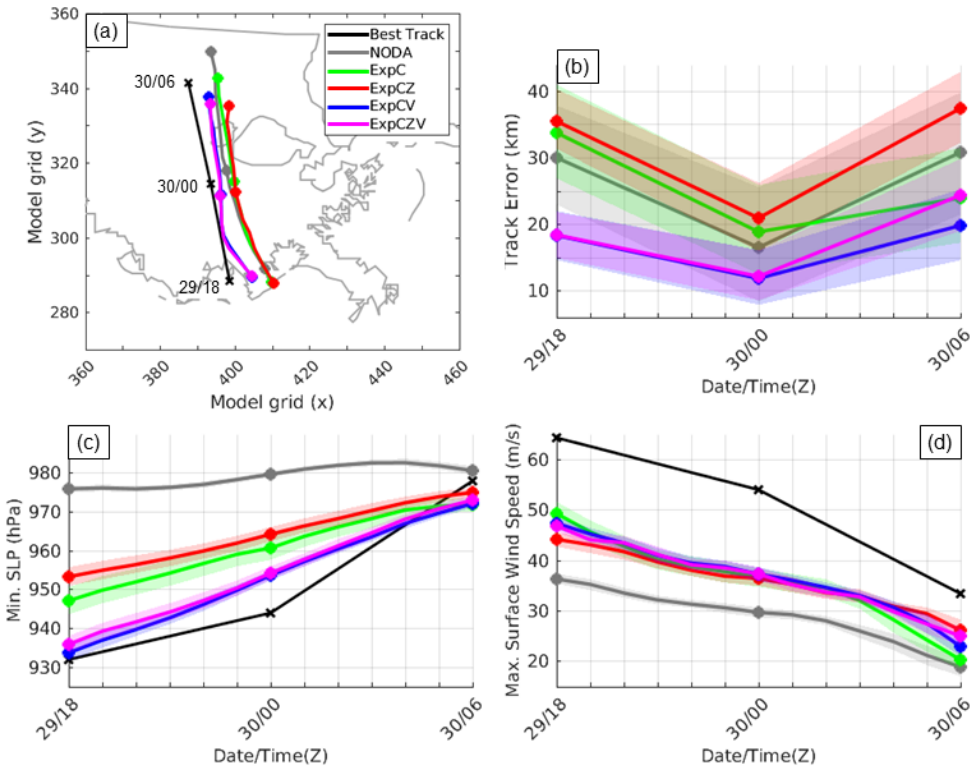

FIG. 11. Ensemble mean forecasts of (a) track, (b) track error, (c) minimum sea level pressure, and (d) maximum surface level wind speed from 1800 UTC 29 August to 0600 UTC 30 August 2021, following Hurricane Ida's landfall (post-landfall). The forecasts are verified hourly for (a), (c), and (d), and every 6 hours for (b) given the best track data availability. Shaded areas with matching colors in (b), (c), and (d) represent the 95% confidence ranges calculated with bootstrap resampling.

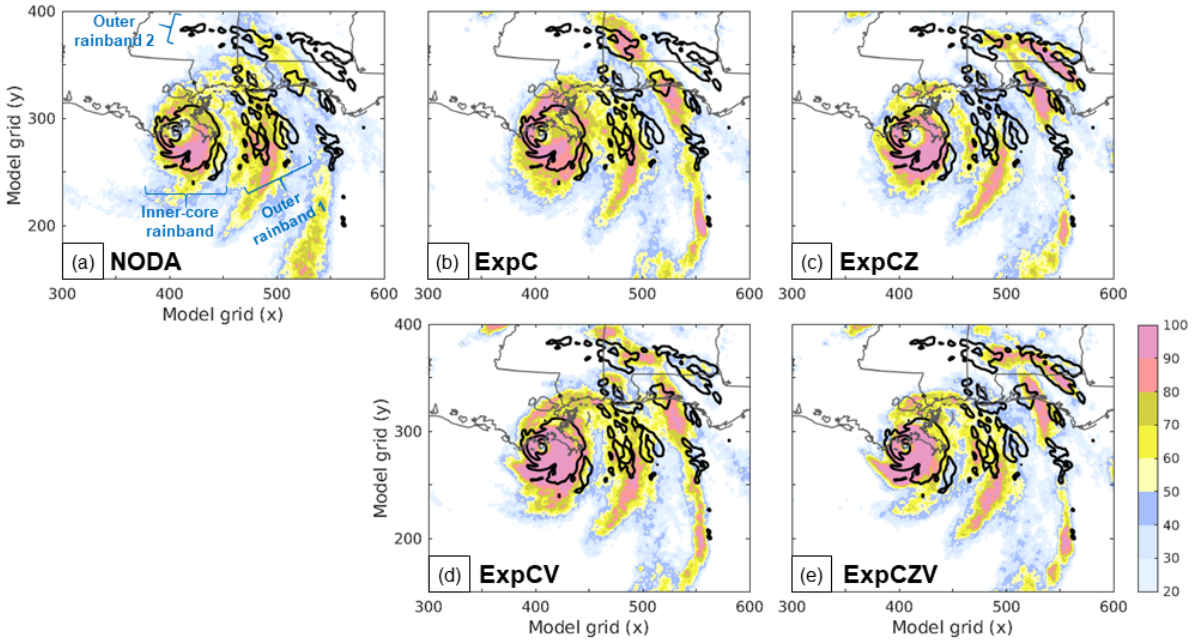

FIG. 12. The ensemble probability (%) of the forecast composite reflectivity exceeding 30 dBZ at 1700 UTC 29 August 2021 (5 minutes after the observed landfall) for experiments (a) NODA, (b) ExpC, (c) ExpCZ, (d) ExpCV, and (e) ExpCZV. The MRMS observed 30-dBZ reflectivity is overlaid in black contours.

2) PRECIPITATION FORECASTING EVALUATION

Figure 12 evaluates the predicted hurricane-associated convection around the landfall time based on the ensemble probability (EP; Schwartz et al. 2010) of the composite reflectivity. Compared with NODA, all DA experiments exhibit notably reduced uncertainty in forecasting the occurrence of significant convective activities, as evidenced by the decrease in areas with low EP values. This reduction mainly results from more accurate track forecasts, as discussed earlier.

Experiments assimilating radar data (ExpCZ, ExpCV, and ExpCZV) show higher confidence for convection within the inner-core region than ExpC, with the observed 30-dBZ area largely covered by EP values exceeding 90%. Specifically, experiments assimilating radial velocity data (ExpCV and ExpCZV) produce ensemble forecasts of hurricane center positions closest to the observed eye location (the embedded closed contour), depicted by lower EP values within the inner core rainbands. This highlights the critical role of radial velocity data in improving track forecasts near landfall, consistent with Fig. 11.

For the outer rainbands, especially those located northeast of the TC center, different DA experiments demonstrate varying degrees of improvement. When assimilating conventional data only (ExpC), the EP in the first outer rainband is slightly lower than in NODA, while the second outer rainband is better captured with significantly higher EP, except near the Alabama-Florida border. With assimilation of additional radial velocity (ExpCV), forecasts of convection near the coastal areas of Mississippi and Alabama and the outermost rainband are further improved. Meanwhile, assimilating reflectivity data (ExpCZ and ExpCZV) greatly increases confidence in forecasting the outermost rainband, suggesting the beneficial impact of reflectivity DA on forecasting specific rainband structures. However, reflectivity DA also leads to reduced EP values for convective activities in some areas, such as near the Mississippi-

Alabama border, large portions of the first outer rainband, and the east to south portion of the second outer rainband, when comparing ExpCZ (ExpCZV) with ExpC (ExpCV). This reduction in forecast convective activity likely reflects not only the generally lower TC intensity near landfall (Fig. 9), which limits the storm's ability to sustain deep convection, but also the influence of environmental stability and the selected model physics on convective development.

Landfall-period precipitation forecasts are evaluated using 4-km Stage IV rainfall products (Nelson et al. 2016) within the defined domain (920 km × 800 km, see Fig. 2). Forecast rainfall fields are conservatively interpolated to the stage IV grid for grid-to-grid quantitative evaluation. Figure 13a-e shows neighborhood ensemble probabilities (NEP; Schwartz et al. 2010) of 2-h rainfall accumulation exceeding 5.08 mm (0.2 inches) between 1500 and 1700 UTC 29 August 2021, approximately 2 hours prior to landfall (1655 UTC). NEP is calculated using a 12-km neighborhood radius and smoothed with a two-dimensional 4-km Gaussian filter (Brooks et al. 1998). The observed rainfall (≥ 5.08 mm) mainly occurs in the hurricane inner core and its northeast quadrant, aligning with convective rainbands previously discussed in Fig. 12.

In the NODA experiment (Fig. 13a), the rainfall associated with the hurricane inner core is generally well captured, while forecasts of outer rainbands are inadequate, likely due to large track errors. Assimilation of conventional data only (ExpC, Fig. 13b) markedly improve forecasts of outer rainbands along the Mississippi-Alabama coastline, likely due to improved track forecasts. Additional reflectivity assimilation (ExpCZ, Fig. 13c) further enhances the forecasts of distant rainbands over northwestern Florida, notably outperforming ExpCV (Fig. 13d) in the outermost rainband despite relatively less accurate track forecast. This highlights that rainfall forecast skill, especially in the outer rainbands, depends on more than just TC track accuracy.

Quantitative assessment using ensemble-mean the equitable threat score (ETS) at the 5.08-mm threshold is presented in Fig. 13f, evaluated for different neighborhood radii following Clark et al. (2010). ExpCZ consistently achieves the highest scores across all radii, followed by ExpCZV and ExpCV, demonstrating the value of radar DA. The advantage of ExpC over NODA is limited to very small neighborhood radii (< 4 km). Due to the wide dispersion in TC center positions among ensemble members, NODA significantly benefits from larger neighborhood radii, as evidenced by the steep increase in ETS with radius expansion.

In the 6-hour post-landfall forecast period, all data assimilation (DA) experiments better capture heavy rainfall (exceeding 76.2 mm) near the hurricane center compared to NODA (Fig. 14), which substantially underpredicts both the intensity and spatial coverage of precipitation. Among the DA experiments, ExpCV and ExpCZV exhibit the highest forecast confidence, with NEP exceeding 90% and closely matching observations. In contrast, ExpC and ExpCZ show weaker performance, though ExpC provides more accurate rainfall coverage than ExpCZ.

These differences are closely tied to the accuracy of storm track forecasts and their influence on inner-core rainfall placement. The improved performance of ExpCV and ExpCZV reflects their better-constrained TC positions, enabled by radial velocity assimilation. In comparison, the larger ensemble spread in storm position in ExpC leads to a more diffuse NEP signal. Meanwhile, ExpCZ, which assimilates reflectivity but not radial velocity, produces a slower-moving TC forecast (Fig. 10), shifting the peak NEP offshore and away from the observed maximum. These spatial rainfall differences are further supported by the ETS verification (Fig. 14f), where ExpCV and ExpCZV achieve the highest scores across most neighborhood radii,

reinforcing the advantages of radial velocity assimilation in capturing heavy post-landfall rainfall.

Overall, the comparison between pre- and post-landfall periods reveals distinct differences in the relative benefits of assimilating reflectivity and radial velocity data. During the 2-hour pre-landfall period (Fig. 13), assimilating reflectivity data yields the most notable improvement, especially in capturing outer rainbands. This is evidenced by ExpCZ achieving the highest ETS values across all neighborhood radii (Fig. 13f), outperforming even the radial velocity assimilated experiments. The short lead time and strong correlation between reflectivity and precipitation contribute to these results as the better analyzed cloud hydrometeors within the rainbands can directly impact subsequent precipitation within a relatively short period. Without direct updating hydrometeors, precipitation in ExpC can only develop through model spin-up along the other updated state variables. In contrast, during the 6-hour post-landfall period (Fig. 14), assimilation of radial velocity becomes more impactful. ExpCV and ExpCZV outperform other experiments in both NEP and ETS metrics (Fig. 14f), highlighting the positive impacts of improved hurricane circulation analysis and improved track forecasts in accurately placing inner-core and rainband. These results suggest that reflectivity assimilation is most beneficial for short-range rainfall prediction during active convection, whereas radial velocity assimilation provides greater value over longer lead times by improving hurricane structure and track forecast accuracy which affect subsequent precipitation forecast skill.

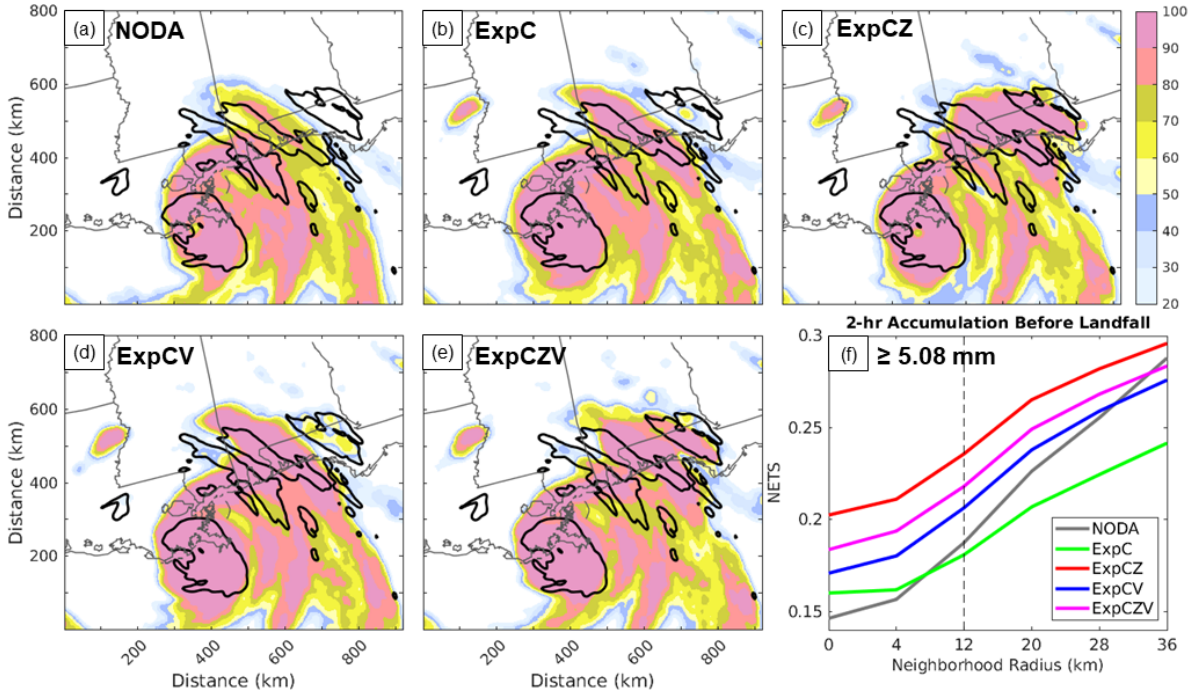

Fig. 13. Neighborhood ensemble probability (%) of 2-h accumulated rainfall forecasts exceeding 5.08 mm (0.2 inches), valid between 1500 UTC and 1700 UTC 29 August 2021, for experiments (a) NODA, (b) ExpC, (c) ExpCZ, (d) ExpCV, and (e) ExpCZV; the same period observed MRMS stage IV rainfall accumulation ≥ 5.08 mm is overlaid in black contours. (f) Ensemble averaged neighborhood ETSs of 2-h forecast rainfall accumulation at a 5.08-mm threshold as a function of neighborhood radius for all experiments denoted by different colors; the dashed line indicates the 12-km neighborhood radius used for NEP.

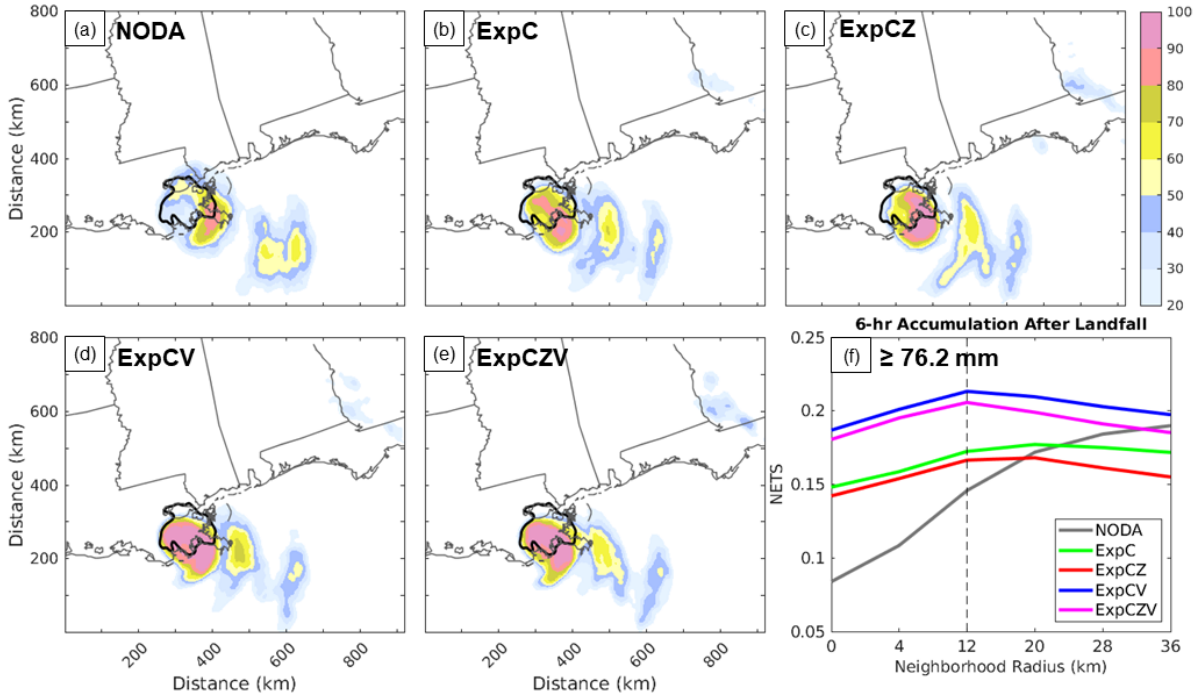

Fig. 14. As in Fig. 13, except for 6-h accumulated rainfall forecasts exceeding 76.2 mm (3.0 inches), valid between 1700 UTC and 2300 UTC 29 August 2021.

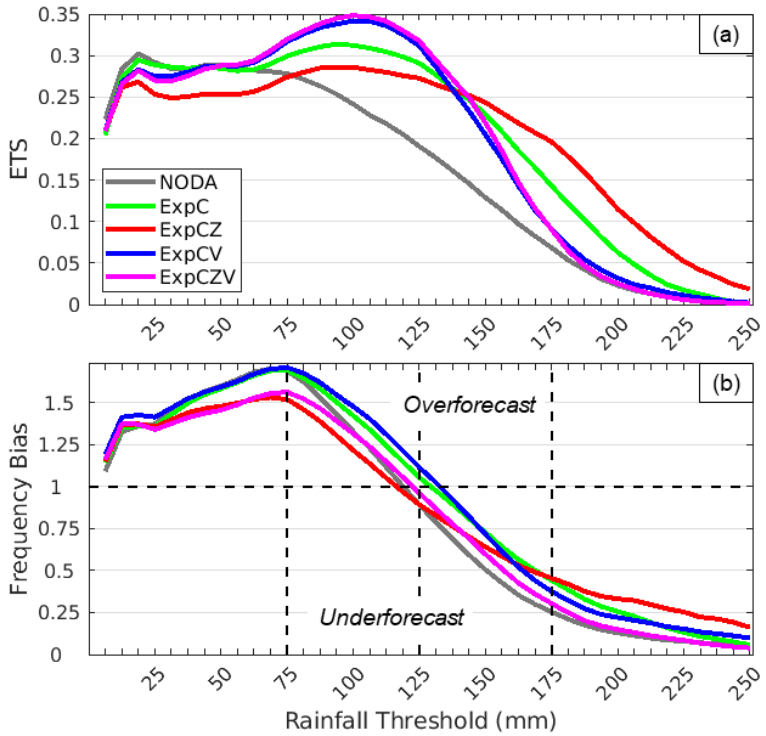

FIG. 15. Ensemble-averaged (a) ETS and (b) frequency bias of 12-h rainfall accumulation forecasts, valid between 1500 UTC 29 August and 0300 UTC 30 August 2021, for different experiments as a function of thresholds calculated in a 6.35-mm (0.25-in) interval starting at 6.35 mm/12 hour.

In addition to the short-term differences in radar DA impact before and after landfall, it is also important to assess the cumulative effects on rainfall forecast skills over a longer period. Figure 15 presents the 12-hour accumulated precipitation forecast verification, using ensemble-averaged ETS (Fig. 15a) and frequency bias (Fig. 15b) as a function of rainfall intensity

thresholds. As shown in Fig. 15a, all DA experiments outperform the NODA baseline across nearly all thresholds, with the largest improvements found in the moderate rainfall range between 50 and 150 mm. Within this range, ExpCV and ExpCZV achieve the highest ETS values, suggesting that radial velocity assimilation enhances forecast accuracy by better constraining the storm track and inner-core structure. ExpC exhibits intermediate skill, while ExpCZ consistently underperforms relative to other DA experiments at these thresholds. This relative underperformance of ExpCZ can be linked to its generally smaller rain area predicted among ensemble members despite locally stronger precipitation intensities (not shown). In addition, the slower storm motion tends to concentrate rainfall closer to the storm center with reduced organized rainfall coverage resulting from the absence of radial velocity assimilation for dynamical balance. These results highlight the benefit of radial wind data in improving mid-range precipitation forecasts.

At higher thresholds above 150 mm, however, the relative ranking changes. While all DA experiments maintain some advantage over NODA, the skill differences diminish. Notably, ExpCZ achieves the highest ETS values up to the 250-mm threshold, outperforming the other DA experiments in capturing localized extreme rainfall. This advantage is likely related to its slower storm motion, which increases inland rainfall accumulation. In contrast, ETS values for ExpCV and ExpCZV decline more rapidly beyond 150 mm and converge toward NODA beyond ~190 mm, suggesting limited capability in forecasting extreme rainfall despite their strong performance at lower thresholds.

Figure 15b further illustrates the systematic forecast biases. Across all experiments, forecasts show overprediction (bias > 1) for thresholds below ~125 mm and underprediction (bias < 1) at higher thresholds. For light to moderate rainfall (25~125 mm), ExpCV and ExpC exhibit the strongest overforecasting tendencies, with bias values approaching 1.7 near 75 mm. In contrast, ExpCZ and ExpCZV produce more conservative forecasts in this range, with bias values closer to unity. ExpCZV exhibits lower bias than ExpCV in the 25~125-mm range, despite comparable ETS values, suggesting a more balanced depiction of rainfall intensity when both reflectivity and radial velocity are assimilated.

At higher thresholds, frequency bias declines for all experiments. Among them, ExpCZ maintains the highest bias beyond 175 mm, indicating the least under-forecasting and aligning with its superior ETS performance at heavy rainfall thresholds. By contrast, ExpCZV exhibits the steepest bias decline beyond 150 mm, with values approaching NODA's levels, suggesting reduced effectiveness in capturing extreme rainfall accumulation.

5. Summary and discussion

This study demonstrates the benefits of assimilating radar observations using newly-established LETKF capabilities within the JEDI framework for improving short-range ensemble forecasts of landfalling Hurricane Ida (2021) with a HAFS-like configuration. In addition to a no-DA control, four DA experiments were conducted with hourly cycling on a 3-km FV3 model domain: a baseline experiment assimilating only conventional observations, and three variants additionally incorporating radar reflectivity and radial velocity, either individually or jointly. This design enabled assessment of how different observation types contribute to improved hurricane analyses and forecasts for potential operational adoption.

Results from the DA cycling phase show that assimilating conventional observations alone improves the near-surface wind and pressure fields compared to the no-DA experiment, while radar data provide additional and distinct benefits. Radar reflectivity assimilation results in a slight contraction of inner core, but has limited impact on surface wind strength, indicating

weak correlations between reflectivity and kinematic fields. Assimilating radial velocity, on the contrary, strengthens inner-core circulation and vertical structures. leading to more accurate track and intensity forecasts that further improve the and a warmer core.

During the subsequent free-forecast period, all DA experiments provide continued forecast improvements over NODA, particularly in track and intensity. Radial velocity assimilation leads to the most accurate landfall location forecasts, associated with smaller ensemble spread and improved representation of the large-scale steering flow. These improvements persist during the free forecasts up to 12 hours after landfall, with the lowest MSLP maintained in the assimilating radial velocity experiments. This indicates that better-constrained inner-core structure supports sustained forecast accuracy in TC intensity.

For the precipitation forecast, radar DA provides clear benefits at different stages of storm evolution. Assimilating reflectivity data greatly improves spatial coverage and ensemble confidence of pre-landfall rainfall forecasts, particularly in capturing outer rainbands. In contrast, post-landfall heavy rainfall prediction benefits more from radial velocity assimilation, as improved track direction and speed lead to more accurate positioning of inland rainfall. This finding is consistent with Marchok et al. (2007), who emphasized that track direction and translation speed are the most important predictors of TC rainfall forecast accuracy.

In summary, this study tests and validates newly implemented capabilities to assimilate coastal ground-based WSR-88D radar reflectivity and radial velocity data within LETKF algorithm of the JEDI DA framework, which is planned to be adopted for the future versions of operational hurricane forecasting system HAFS of NOAA. It also demonstrates the value of radar data assimilation for improving ensemble-based hurricane forecasting within a HAFS-like configuration. Radar reflectivity and radial velocity provide complementary benefits: reflectivity enhances pre-landfall rainfall forecasts, especially for outer rainbands, while radial velocity substantially improves the analysis and prediction of storm structure, intensity, and track. The combination experiment assimilating all data types yields the most comprehensive improvements across all evaluation metrics, highlighting how integrating multiple radar data types can enhance both structural and hydrometeorological aspects of tropical cyclone forecasting. These findings are consistent with prior radar DA studies (e.g., Zhao and Xue 2009; Dong and Xue 2013; Zhao and Jin 2008), and emphasize the operational value of assimilating high-resolution radar observations near landfall to enhance short-range forecasts and support timely decision-making for disaster preparedness.

It should be noted that the results presented here are obtained using a simplified HAFS-like configuration for computational feasibility, rather than the full operational HAFS that features moving nests with finer resolutions. While this limits direct applicability to operations, the findings provide an important first step toward implementing and evaluating radar data assimilation within the JEDI framework for HAFS. Although not explicitly tested in this study, additional features in HAFS such as storm-following nests, multiscale DA, and ocean coupling should not alter the overall conclusions. The demonstrated benefits of radar DA suggest practical value in guiding the future development of the operational deterministic 4DEnVAR system. Specifically, ensembles updated by radar data assimilation using LETKF can provide more accurate flow-dependent background error covariances, which are critical to effective 4DEnVAR performance within the HAFS framework.

Although the present study demonstrates promising results, it is intentionally focused on a single case with a short forecast range, as radar data assimilation primarily influences the very short-range forecasts within the first 12 hours after analysis. Broader evaluations involving additional cases and longer forecast periods will be needed to assess the generality, statistical

robustness, and cost-benefit of the implemented approach. Moreover, the increased computational cost associated with high-resolution high-frequency cycled ensemble DA must be carefully assessed when considering operational implementation of high-density radar DA capabilities. Finally, we point out that in a sense, using NODA experiment as the benchmark to assess the impact of assimilating additional data at later times is not strictly fair, since the initial condition of NODA is 9 hours earlier than the DA experiments that assimilate the final batch of data at 1500 UTC. However, comparing the relative performance of experiments assimilating different data types is the more important goal of this study, while NODA is used merely as a reference. The differences between the DA experiments and NODA serve to show that the assimilation of new observations does improve the hurricane analysis and subsequent forecast, and in what ways. With these direct radar data assimilation capabilities now available in the JEDI repository, this study provides a documented example of their application to tropical cyclone forecasting, facilitating further evaluation and development within the JEDI framework.

Acknowledgments. This study was supported by the NOAA Grant NA21OAR4590171 of the Joint Technology Transfer Initiative (JTTI) Program. Special thanks to Dr. Zhan Zhang of NOAA/EMC for valuable consultation on the configuration of the HAFS suite available in the UFS. The supercomputer XSEDE Stampede2 at the university of Texas Advanced Computing Center (TACC) was utilized for this study.

Data Availability Statement:

The JEDI-FV3 bundle (version 1.0.0) used in this study is openly available at https://github.com/JCSDA. The UFS SRW App (public-v2.0.0) employed for the model simulations can be accessed at https://github.com/ufs-community/ufs-srweather-app. The source data for the MRMS composite reflectivity and NEXRAD Level II radial velocity are publicly available at https://mrms.nssl.noaa.gov/ and

https://www.ncei.noaa.gov/products/radar/next-generation-weather-radar, respectively. For reproducibility, a subset of the data used in this study, including the processed conventional and radar observations in netCDF format and the YAML configuration files for performing the JEDI LETKF, is permanently archived at the Harvard Dataverse: https://doi.org/10.7910/DVN/MTVSOT.

REFERENCES

Alaka, G. J., Jr., and Coauthors, 2024: Lifetime performance of the operational Hurricane Weather Research and Forecasting model (HWRF) for North Atlantic tropical cyclones *Bull. Amer. Meteor. Soc.*, **105,** E932-E961, https://doi.org/10.1175/BAMS-D-23-0139.1.

Arakawa, A., and W. H. Schubert, 1974: Interaction of a cumulus cloud ensemble with the large-scale environment, Part I. *J. Atmos. Sci.*, **31,** 674-701, https://doi.org/10.1175/1520-0469(1974)031<0674:IOACCE>2.0.CO;2.

Brooks, H. E., M. Kay, and J. A. Hart, 1998: Objective limits on forecasting skill of rare events. *19th Conf. on Severe Local Storms*, A. M. Soc., Ed., 552-555, https://www.nssl.noaa.gov/users/brooks/public_html/papers/sls19.pdf.

Chen, S. S., J. F. Price, W. Zhao, M. A. Dpnelan, and E. J. Walsh, 2007: The CBLAST-hurricane program and the next-generation fully coupled atmosphere-wave-ocean models

for hurricane research and prediction. *Bull. Amer. Meteor. Soc.*, **88,** 311-318, https://doi.org/10.1175/BAMS-88-3-311.

Clark, A. J., W. A. Gallus, and M. L. Weisman, 2010: Neighborhood-based verification of precipitation forecasts from convection-allowing NCAR WRF model simulations and the operational NAM. *Wea. Forecasting*, **25,** 1495-1509, https://doi.org/10.1175/2010WAF2222404.1.

Davis, C., and Coauthors, 2008: Prediction of landfalling hurricanes with the Advanced Hurricane WRF model. *Mon. Wea. Rev.*, **136,** 1990-2005, https://doi.org/10.1175/2007MWR2085.1.

Dong, J., and M. Xue, 2013: Assimilation of radial velocity and reflectivity data from coastal WSR-88D radars using an ensemble Kalman filter for the analysis and forecast of landfalling hurricane Ike (2008). *Quart. J. Roy. Meteor. Soc.*, **139,** 467-487, https://doi.org/10.1002/qj.1970.

Dong, J., and Coauthors, 2020: The evaluation of real-time Hurricane Analysis and Forecast System (HAFS) Stand-Alone Regional (SAR) model performance for the 2019 Atlantic hurricane season. *Atmosphere*, **11,** 617, https://doi.org/10.3390/atmos11060617.

Fierro, A. O., R. F. M. Rogers, Frank D., and D. S. Nolan, 2009: The impact of horizontal grid spacing on the microphysical and kinematic structures of strong tropical cyclones simulated with the WRF-ARW model. *Mon. Wea. Rev.*, **137,** 3717-3743, https://doi.org/10.1175/2009MWR2946.1.

Gao, J., M. Xue, S. Y. Lee, A. Shapiro, Q. Xu, and K. K. Droegemeier, 2006: A three-dimensional variational single-Doppler velocity retrieval method with simple conservation equation constraint. *Meteo. Atmos. Phys.*, **94,** 11-26, https://doi.org/10.1007/s00703-005-0170-7.

Gaspari, G., and S. E. Cohn, 1999: Construction of correlation functions in two and three dimensions. *Quart. J. Roy. Meteor. Soc.*, **125,** 723-757, https://doi.org/10.1002/qj.49712555417.

Green, T., X. Wang, and X. Lu, 2022: Impact of assimilating ground-based and airborne radar observations for the analysis and prediction of the eyewall replacement cycle of Hurricane Matthew (2016) using the HWRF hybrid 3DEnVar system. *Mon. Wea. Rev.*, **150,** 1157-1175, https://doi.org/10.1175/MWR-D-21-0234.1.

Han, J., and C. S. Bretherton, 2019: TKE-based moist eddy-diffusivity mass-flux (EDMF) parameterization for vertical turbulent mixing *Wea. Forecasting*, **34,** 869-886, https://doi.org/10.1175/WAF-D-18-0146.1.

Hazelton, A., G. J. Alaka, Jr., M. S. Fischer, R. Torn, and S. B. Goldenberg, 2023: Factors influencing the track of Hurricane Dorian (2019) in the West Atlantic: Analysis of a HAFS ensemble *Mon. Wea. Rev.*, **151,** 175-192, https://doi.org/10.1175/MWR-D-22-0112.1.

Hazelton, A., and Coauthors, 2021: 2019 Atlantic hurricane forecasts from the global-nested Hurricane Analysis and Forecast System: Composite statistics and key events *Wea. Forecasting*, **36,** 519-538, https://doi.org/10.1175/WAF-D-20-0044.1.

Hazelton, A., and Coauthors, 2022: Performance of 2020 real-time Atlantic hurricane forecasts from high-resolution global-nested hurricane models: HAFS-globalnest and

GFDL T-SHiELD. *Wea. Forecasting*, **37,** 143-161, https://doi.org/10.1175/WAF-D-21-0102.1.

Hsiao, L.-F., and Coauthors, 2012: Application of WRF 3DVAR to operational typhoon prediction in Taiwan: Impact of outer loop and partial cycling approaches. *Wea. Forecasting*, **27,** 1249-1263, https://doi.org/10.1175/WAF-D-11-00131.1.

Hunt, B. R., E. J. Kostelich, and I. Szunyogh, 2007: Efficient data assimilation for spatiotemporal chaos: A local ensemble transform Kalman filter. *Physica D*, **230,** 112-126, https://doi.org/10.1016/j.physd.2006.11.008.

Jacobs, N. A., 2021: Open innovation and the case for community model development. *Bull. Amer. Meteor. Soc.*, **102,** E2002–E2011, https://doi.org/10.1175/BAMS-D-21-0030.1.

Kim, H.-S., and Coauthors, 2014: Performance of ocean simulations in the coupled HWRF–HYCOM model *J. Atmos. Ocean. Technol.*, **31,** 545-559, https://doi.org/10.1175/JTECH-D-13-00013.1.

Kurihara, Y., M. A. Bender, and R. J. Ross, 1993: An initialization scheme of hurricane models by vortex specification. *Mon. Wea. Rev.*, **121,** 2030-2045, https://doi.org/10.1175/1520-0493(1993)121<2030:AISOHM>2.0.CO;2.

Labriola, J., Y. S. Jung, C. S. Liu, and M. Xue, 2021: Evaluating forecast performance and sensitivity to the GSI EnKF data assimilation configuration for the 28-29 May 2017 mesoscale convective system case. *Wea. Forecasting*, **36,** 127-146, https://doi.org/10.1175/WAF-D-20-0071.1.

Li, T.-H., X. Wang, and X. Lu, 2024: Impact of direct radar reflectivity data assimilation on the simulation of mesoscale descending inflow and secondary eyewall formation in Hurricane Matthew (2016). *Geophys Res Lett*, **51,** 10, https://doi.org/10.1029/2023GL106514.

Liu, L., and Coauthors, 2023: Impact of assimilating satellite and glider observations on Hurricane Isaias (2020) forecast using marine JEDI. *Wea. Forecasting*, **38,** 1807-1826, https://doi.org/10.1175/WAF-D-22-0014.1.

Lord, S. J., H. E. Willoughby, and J. M. Piotrowicz, 1984: Role of a parameterized ice-phase microphysics in an axisymmetric, nonhydrostatic tropical cyclone model. *J. Atmos. Sci.*, **41,** 2836-2848, https://doi.org/10.1175/1520-0469(1984)041<2836:ROAPIP>2.0.CO;2.

Lu, X., X. Wang, M. Tong, and V. Tallapragada, 2017: GSI-based, continuously cycled, dual-resolution hybrid ensemble–variational data assimilation system for HWRF: System description and experiments with Edouard (2014). *Mon. Wea. Rev.*, **145,** 4877-4898, https://doi.org/10.1175/MWR-D-17-0068.1.

Marchok, T., R. Rogers, and R. Tuleya, 2007: Validation schemes for tropical cyclone quantitative precipitation forecasts: Evaluation of operational models for U.S. landfalling cases. *Wea. Forecasting*, **22,** 726-746, https://doi.org/10.1175/WAF1024.1.

Miyoshi, T., S. Yamane, and T. Enomoto, 2007: Localizing the error covariance by physical distances within a local ensemble transform Kalman filter (LETKF). *SOLA*, **3,** 89-92, https://doi.org/10.2151/sola.2007-023.

Mlawer, E. J., S. J. Taubman, P. D. Brown, M. J. Iacono, and S. A. Clough, 1997: Radiative transfer for inhomogeneous atmospheres: RRTM, a validated correlated-k model for the longwave. *J. Geophys. Res.*, **102,** 16663-16682, https://doi.org/10.1029/97JD00237.

Nelson, B. R., O. P. Prat, D. J. Seo, and E. Habib, 2016: Assessment and implications of NCEP stage IV quantitative precipitation estimates for product intercomparisons. *Wea. Forecasting*, **31,** 371-394, https://doi.org/10.1175/WAF-D-14-00112.1.

Niu, G. Y., and Coauthors, 2011: The community Noah land surface model with multiparameterization options (Noah-MP): 1. Model description and evaluation with local-scale measurements. *J. Geophys. Res.*, **116,** 19, https://doi.org/10.1029/2010JD015139.

Park, J., M. Xue, and C. Liu, 2023: Implementation and testing of radar data assimilation capabilities within the Joint Effort for Data Assimilation Integration framework with ensemble transformation Kalman filter coupled with FV3-LAM model. *Geophys Res Lett*, **50,** 9, https://doi.org/10.1029/2022GL102709.

Pondeca, M. S. F. V. D., and Coauthors, 2011: The real-time mesoscale analysis at NOAA's National Centers for Environmental Prediction: Current status and development. *Wea. Forecasting*, **26,** 593-612, https://doi.org/10.1175/WAF-D-10-05037.1.

Putman, W. M., and S.-J. Lin, 2007: Finite-volume transport on various cubed-sphere grids. *Journal of Computational Physics*, **227,** 55-78, https://doi.org/10.1016/j.jcp.2007.07.022.

Schwartz, C. S., and Coauthors, 2010: Toward improved convection-allowing ensembles: Model physics sensitivities and optimizing probabilistic guidance with small ensemble membership. *Weather and Forecasting*, **25,** 263-280, https://doi.org/10.1175/2009WAF2222267.1.

Snook, N., M. Xue, and Y. S. Jung, 2015: Multiscale EnKF assimilation of radar and conventional observations and ensemble forecasting for a tornadic mesoscale convective system. *Monthly Weather Review*, **143,** 1035-1057, https://doi.org/10.1175/MWR-D-13-00262.1.

Tremolet, Y., and T. Auligne, 2020: The Joint Effort for Data Assimilation Integration (JEDI). *JCSDA Quarterly*, No. 66, Joint Center for Satellite Data Assimilation, College Park, MD, 61-65, https://doi.org/10.25923/rb19-0q26.

Uccellini, L. W., W. R. Spinrad, D. M. Koch, C. N. McLean, and W. M. Lapenta, 2022: EPIC as a catalyst for NOAA's future Earth prediction system. *Bull. Amer. Meteor. Soc.*, **103,** E2246–E2264, https://doi.org/10.1175/BAMS-D-21-0061.1.

Wang, Y., and Z. Pu, 2021: Assimilation of radial velocity from coastal NEXRAD into HWRF for improved forecasts of landfalling hurricanes. *Wea. Forecasting*, **36,** 587-599, https://doi.org/10.1175/WAF-D-20-0163.1.

Weng, Y., and F. Zhang, 2012: Assimilating airborne Doppler radar observations with an ensemble Kalman filter for convection-permitting hurricane initialization and prediction: Katrina (2005) *Mon. Wea. Rev.*, **140,** 841-859, https://doi.org/10.1175/2011MWR3602.1.

Whitaker, J. S., and T. M. Hamill, 2012: Evaluating methods to account for systemerrors in ensemble data assimilation. *Mon. Wea. Rev.*, **140,** 3078-3089, https://doi.org/10.1175/MWR-D-11-00276.1.

Wu, W. S., R. J. Purser, and D. F. Parrish, 2002: Three-dimensional variational analysis with spatially inhomogeneous covariances. *Mon. Wea. Rev.*, **130,** 2905-2916, https://doi.org/10.1175/1520-0493(2002)130<2905:TDVAWS>2.0.CO;2.

Zhang, F. Q., Y. H. Weng, J. A. Sippel, Z. Y. Meng, and C. H. Bishop, 2009: Cloud-resolving hurricane initialization and prediction through assimilation of Doppler radar

observations with an ensemble Kalman filter. *Mon. Wea. Rev.*, **137,** 2105-2125, https://doi.org/10.1175/2009MWR2645.1.

Zhang, J., and Coauthors, 2016: Multi-Radar Multi-Sensor (MRMS) quantitative precipitation estimation: Initial operating capabilities. *Bull. Amer. Meteor. Soc.*, **97,** 621-638, https://doi.org/10.1175/BAMS-D-14-00174.1

Zhang, S., and Z. Pu, 2019: Numerical simulation of rapid weakening of Hurricane Joaquin with assimilation of high-definition sounding system dropsondes during the Tropical Cyclone Intensity Experiment: Comparison of three- and four-dimensional ensemble–variational data assimilation. *Wea. Forecasting*, **34,** 521-538, https://doi.org/10.1175/WAF-D-18-0151.1.

Zhao, K., and M. Xue, 2009: Assimilation of coastal Doppler radar data with the ARPS 3DVAR and cloud analysis for the prediction of Hurricane Ike (2008). *Geophys Res Lett*, **36**, https://doi.org/10.1029/2009GL038658.

Zhao, Q. Y., and Y. Jin, 2008: High-resolution radar data assimilation for hurricane Isabel (2003) at landfall. *Bull. Amer. Meteor. Soc.*, **89,** 1355-1372, https://doi.org/10.1175/2008BAMS2562.1.